Effects of Fe Dopant on Structural, Optical and Electrical Properties of NiTiO₃ Materials

Tran Vu Diem Ngoc[1], Luong Huu Bac[2],*

[1]School of Materials Science and Engineering, Hanoi University of Science and Technology, Hanoi, Vietnam
[2]School of Engineering Physics, Hanoi University of Science and Technology, Hanoi, Vietnam
*Email: bac.luonghuu@hust.edu.vn

Abstract

In this study, the effects of Fe dopant on the structural, optical, and electrical properties of NiTiO₃ materials prepared by sol-gel method were investigated. The prepared powders were investigated through X-ray diffraction, Raman scattering, scanning electron microscope, UV-visible absorption, vibrating sample magnetometer, electrical measurement to explore the structural, ferromagnetic, and electrical properties. The single-phase $Ni_{1-x}Fe_xTiO_3$ (x = 0, 0.05 and 0.10) materials were obtained. Doping of Fe into NiTiO₃ lead to the decreasing of lattice parameter and increased the particle size compared to the undoped sample. Ferroelectric and ferromagnetic properties of all Fe-doped NiTiO₃ ceramics have been investigated at room temperature. The ferromagnetic hysteresis loop of the Fe-doped NiTiO₃ sample at room temperature is due to the formation of oxygen vacancies and their associated exchange interaction. Ferroelectric properties of Fe doped samples were decreased with the increase of Fe concentration. This can be due to the Fe dopant into NiTiO₃ material. The Fe dopant caused to increase the conductivity of NiTiO₃ sample which resulted in a decrease in ferroelectric parameters.

Keywords: NiTiO₃, ferroelectric properties, conductivity, dopant, ilmenite.

1. Introduction

Enhancement of ferromagnetic properties in ferroelectric materials has been studied in order to expand practical applications of ferroelectric materials. For ferroelectric materials, enhancement of magnetic properties can be done by doping transition metal materials into ferroelectric substrates. Many studies have shown that doping transition metals such as Fe, Co, Mn... can change the magnetic properties of materials. Lihong Yang *et. al.* investigated the effect of Fe dopant on the magnetic properties of BaTiO₃ [1]. The results showed that room temperature hysteresis loops of the $BaTi_{1-x}Fe_xO_3$ samples are observed with doping level *x* from 0.2 and 0.5. The Ms firstly increased and then decreased with increasing doping concentration which indicated the coexistence of ferromagnetism and antiferromagnetism. Xu *et. al.* investigated the room temperature ferromagnetism in Fe-doped BaTiO₃ and predicted the magnetic moment per Fe atom of ~3.05 μ_B [2]. Attaphol Karaphun *et. al.* studied the magnetic properties of Fe-doped SrTiO₃ nanopowders prepared by hydrothermal method [3]. Results showed that the undoped samples behave paramagnetic, whereas the Fe-doped samples are ferromagnetic. It was suggested that the observed ferromagnetism in Fe doped SrTiO₃ originated from the F-center mechanism.

Nickel titanate (NiTiO₃) is a material of the ilmenite family that has been interested in recent research because of its many interesting physico-chemical properties. This material can be tremendously potential for many of applications such as photocatalyst under visible-light irradiation, fuel cells, gas sensor, pigment, and spin electronic devices [4]. NiTiO₃ belongs to the ilmenite type structure with both Ni and Ti processing octahedral coordination and the alternating cation layers occupied by Ni^{2+} and Ti^{4+} alone [5]. NiTiO₃ is a kind of n-type semiconductor with a band gap of round 2.18 eV while the activation energy of single crystal NiTiO₃ is observed in the range from 0.738 eV to 1.06 eV. Bulk NiTiO₃ exhibited the antiferromagnetism with a Neel temperature of 15-22 K [5].

Doping or compositing to modify the properties of NiTiO₃ materials have been investigated and there are a number of reports to dope and composite with NiTiO₃. However, most of the work only concentrated on the structural and optical properties of NiTiO₃ materials. Yi-Jing Lin *et. al.* described the synthesis of the NiTiO₃ containing different amounts of silver by the modified Pechini method. The apparent enhancement in the reduction of methylene blue can be ascribed to simultaneous effects of Ag deposits by acting as electron traps and improving the photocatalytic properties of the Ag-NiTiO₃ in decolorization of methylene blue which was released from the industry-leading to environmental contamination in ecosystem [4]. Fujioka *et al.*

prepared $Ni_{1-x}Co_xTiO_3$ ($0.05 \leq x \leq 0.80$) solid solution using a solid-state technique and studied the structural distortion using Raman analysis [6]. The transition was assigned to mixing of Ni, Co, and Ti cations, resulting in a transition from the ilmenite structure to a disordered structure. Vacant octahedra were suggested to play an important role in the structural transformation. $Fe^{3+}/NiTiO_3$ ferromagnetic nanoparticles were reported by Nayagam Lenin et al [7]. The impedance analysis of ferromagnetic materials explores the ferro-dielectric behavior with enhanced properties of $Fe^{3+}/NiTiO_3$ nanoparticles with an increasing of Fe dopant. The observed results concluded that improved properties of magnetic nanoparticles were found as an influence of nucleation reaction rate with addition of higher Fe content.

In this work, we reported the investigation results of structural, optical and electrical properties of Fe-doped $NiTiO_3$ nanoparticles synthesized using sol-gel method. The Fe doping decreased the optical band gap values from 2.23 eV and 1.79 eV, respectively. Fe doping enhanced the magnetic properties of $NiTiO_3$. However, the increase of conductivity of $NiTiO_3$ with Fe dopant can consequently cause degradation and lossy behavior in ferroelectric properties of $NiTiO_3$.

2. Experiment

2.1. Materials

The Fe-doped $NiTiO_3$ ($Ni_{1-x}Fe_xTiO_3$, x=0, 0.05 and 0.10) nanoparticles were synthesized using the sol-gel technique. The raw materials used consist of tetraisopropoxytitanium (IV) ($C_{12}H_{28}O_4Ti$), nickel nitrate ($Ni(NO_3)_2.6H_2O$), and iron nitrate ($Fe(NO_3)_3.9H_2O$). The citric acid solution ($C_6H_8O_7$) was selected as the solvent. These chemicals were utilized in the synthesis of the samples used with distilled water.

2.2. Sample Preparation

The experimental procedure for the $NiTiO_3$ and Fe-doped $NiTiO_3$ samples was as follows. Firstly, 2 ml of the tetraisopropoxytitanium (IV) was dissolved in citric acid solution at 70 °C. A transparent homogeneous sol was formed after stirring vigorously for 2 h. Then, the 1.96 g nickel nitrate was introduced with mol of Ni equal to mol of Ti for fabricating of $NiTiO_3$. The additional amounts of iron nitrate were added to the solution for preparing Fe-doped $NiTiO_3$ samples. The solutions were stirred around 3-4 h. The solutions were kept stirring around two hours and then heated to around 120 °C to prepare dry gels. The dry gels were ground and calcined from 900 °C for 3 hours.

2.3. Pellet Preparation and Sintering

The obtained powder after calcination was mixed with a small amount of polyvinyl alcohol (PVA, 5%) to constitute a homogeneous mixture. The mixture was dried at 100 °C for 2 h. The resultant mixture was pressed into pellets using a cylindrical steal die of 10 mm in diameter. The powder mixture was pressed with a uniaxial hydraulic press at a pressure of 10^6 N/m².

The sintering procedure is very important to keep the sample to avoid crack which significantly affected the electrical properties of materials. The pressed pellets were heated up to 500 °C with a heating rate of 5 °C/min and a dwell time of 2 h. Then, the temperature continued increasing up to 1200 °C with heating rate of 5 °C/min and dwell time of 5 h in the air atmosphere. After finishing, the pellets were cooled down with natural furnace cooling rate and pellets were taken out of the furnace for analysis.

2.3. Characterization

The morphology of the nanopowders was observed by field emission scanning electron microscope (FE-SEM, JEOL JSM-7600F). The crystalline structures of the samples were characterized by X-ray diffraction (XRD, Philips-X'PertPro) using Cu Kα radiation in 2θ from 20° to 70°. with a step size of 0.02° and a speed of 2°/min. The vibrational and rotational modes in samples were characterized by Raman spectroscopy (JASCO Raman NRS-3000). The optical properties were studied by UV-Vis spectroscopy (JASCO V- 750). The magnetic properties were characterized by vibration samples magnetometer (VSM, Lakeshore 7400) at room temperature.

In order to prepare the sample for electrical measurement, the sintered pellet samples were polished to make a flat and smooth surface. The polished pellets were washed with ethanol by ultrasonic machine and dried at 60 °C for 1 h. A thin layer of silver was coated on both sides of the sintered samples by screen printing technique to make the surface parallel electrodes. The electrode silver deposited samples were then heated at 700 °C for 30 min. DC electrical resistivity was estimated by employing two probe procedures. A P–E hysteresis loop tracer was used to measure the electrical hysteresis loops.

3. Results and Discussion

3.1. XRD Analysis

The X-ray diffraction analysis was used to determine the purity of the synthesized powders. Fig. 1 shows the XRD patterns of $NiTiO_3$ and Fe-doped $NiTiO_3$ samples which were annealed at 900 °C for 3 h. The sharp diffraction peaks and low noise background exhibited that the synthesized powders were crystalline. All samples included the diffraction peaks at 2θ = 24.03°, 32.99°, 35.55°, 40.76°, 49.34°, 53.90°, 57.35°, 62.35°, and 63.97°, and relative intensity were well matched with the standard ICDD-PDF-00-033-0960. These XRD results presented that the synthesized powders belonged to the rhombohedral

crystal structure with R-3 space group. There was no trace of impurity phases or second phases indicating that Fe has successfully substituted Ni into the lattice of $NiTiO_3$. The peak position in XRD pattern shifted to a lower 2θ diffraction angle which is related to the expansion of the lattice parameter. The lattice parameters are calculated from these XRD data using unit cell software. All position of XRD diffraction peak was carefully fitted using the Gaussian curve by OriginLab pro software. The lattice parameter as function of Fe dopant was estimated and shown in Fig. 1(c) and Table 1. The result exhibited that the lattice parameters of $NiTiO_3$ decreased with increase in Fe dopant concentration. These results happened because of different radius of Ni and Fe ion in lattice. The radius of Ni^{2+} ions is bigger than that of Fe^{2+} ions. According to Shannon's report, Ni^{2+} ions have a radius of 0.69Å (in the coordination with VI) while Fe^{2+} ions have a radius of 0.61Å [11].
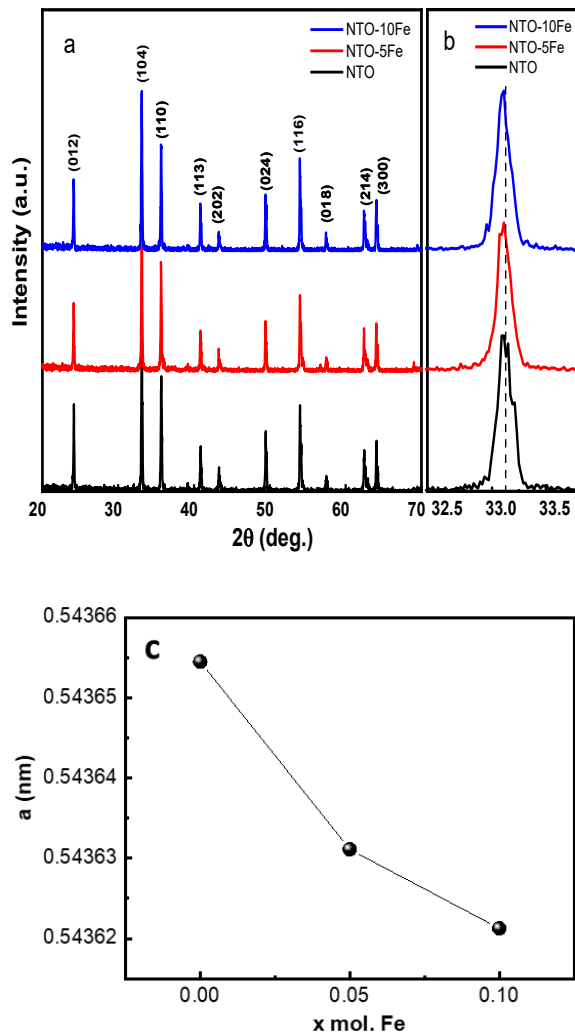
Table 1. Lattice constant and volume of the synthesized Fe doped samples

x	a (Å)	α (^{0})	Volume (Å^3)
0	5.4365	55.08	100.62
0.05	5.4363	55.10	100.65
0.10	5.4362	55.11	100.67

Fig.1(b) shows the magnification of X-ray diffraction patterns of undoped and Fe-doped $NiTiO_3$ samples in 2θ range from 32.5°-33.5°. The zoom-in XRD peaks showed that the peak position of the Fe doped samples slightly shifted toward a lower 2θ value. This result provided evidence that Fe^{2+} cations were incorporated in the lattice structure and replaced on the Ni^{2+} site in lattice.

To analyze the impact of Fe doping on crystal structure stability, the tolerance factor, which is defined for an ABO_3-type ilmenite structure, was calculated as follows

$$t = \frac{1}{3}\left(\frac{(\sqrt{2}+1)R_{O-2}+R_B}{R_{O-2}+R_A}\right) + \frac{\sqrt{2}R_{O-2}}{R_{O-2}+R_B} \qquad (1)$$

where R_A, R_B, and R_O are the ionic radii of A, B, and O^{2-} (1.4 Å), respectively. The tolerance factor for $NiTiO_3$ was 0.9647. The substitution of Fe^{2+} in Ni^{2+} resulted in a slight increase in tolerance factor.

3.2. Morphology and Particle Size

The effect of Fe dopant on the morphology and particle size of synthesized powders were shown in Fig. 2(a)-(c). Overall, the morphology of powders was almost not influenced by Fe dopant. Clearly, the SEM image showed that the surface of sample was non-uniform in size distribution. The grain of all samples was almost irregular shape. The grains are looking like polygonal structures with clear grain boundaries. The morphological texture of the grains is looking smooth and well arranged. Wide distribution in grain size was observed in the SEM image. The $NiTiO_3$ samples had a grain size of around 100-350 nm. However, the grain size of Fe doped $NiTiO_3$ samples was larger and inhomogeneous with higher Fe concentration dopants. The grain sizes for Fe substituted sample are somewhat larger than the undoped sample and this is due to the effect of Fe dopant which helps in grain growth. The average grain size measured in SEM image was around 120 nm to 460 nm for the 10 mol.% Fe doped $NiTiO_3$ sample.

Furthermore, the energy dispersive spectra (EDS) was analyzed to confirm the stoichiometric composition of the synthesized materials which was presented in Fig. 2d. The elemental weight composition percentage is presented in the inset of Fig. 2d. The presence of elements Ni, Ti, Fe, and O in the sample indicated that all chemicals to form the

Fig. 1. a) XRD pattern of Fe doped $NiTiO_3$ samples, b) zoom-in of XRD pattern and c) lattice constant

phase existed in synthesized samples. As can be shown in the figure and the data of weight and atomic percentage compositions, the constituent elemental compositions and the ratios are in line with expected elemental compositions.
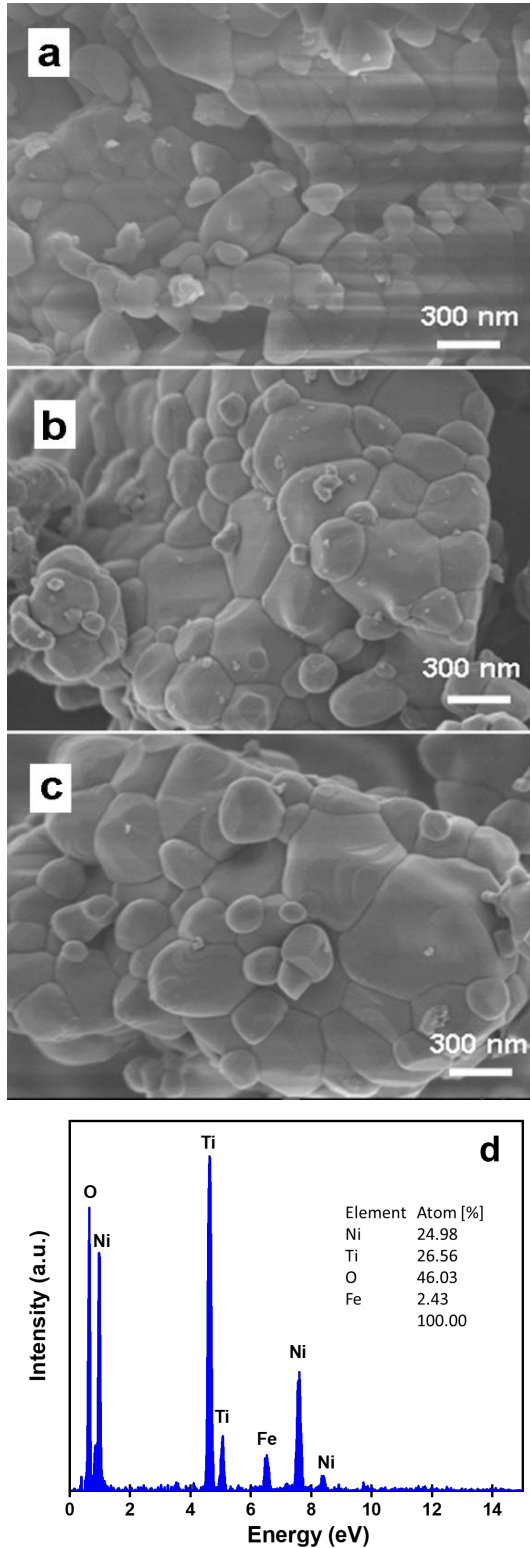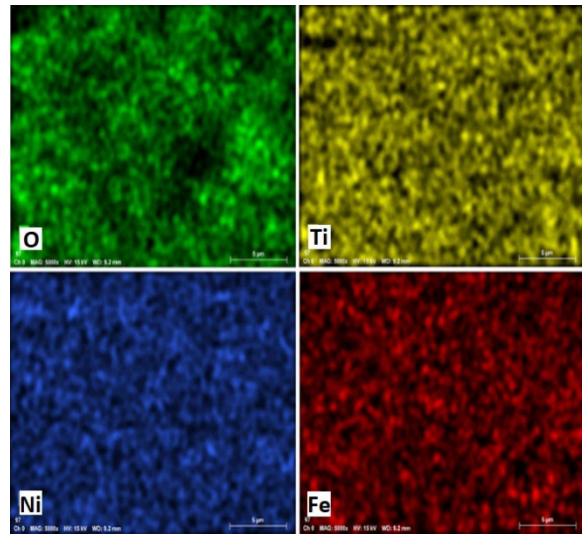

Fig. 3. Energy dispersive X-ray spectroscopy mapping of the Fe-doped $NiTiO_3$ sample.

In order to verify the distribution of the metastable phase, EDS elemental mapping was performed on the Fe doped sample. Fig. 3 showed EDS mapping result of the Fe-doped $NiTiO_3$ sample. The EDS mapping presented a distribution of specific elements which indicated by unique colors. The element maps of Ni, Ti, Fe, and O reveal that all the elements are uniformly distributed in the selected scan area.

3.3. Vibration Analysis

Fig. 4 showed the Raman scattering of $NiTiO_3$ and Fe-doped $NiTiO_3$ samples at room temperature. The theoretical calculation predicted that the optical normal modes of vibrations of $NiTiO_3$ material have the ten active Raman modes $5Ag+ 5Eg$ [8]. In Fig. 4 the ten Raman active modes can be clearly seen which confirmed the ilmenite structure of synthesized $NiTiO_3$ materials. The peak positions were estimated to be consistent with recent calculations for vibration modes activity of $NiTiO_3$ materials by M. A. Ruiz-Preciado *et. al.* [9]. The band located at 720 cm^{-1} was related to the Ti-O-Ti vibration of the crystal structure [9]. The band modes at 617 cm-1 and 690 cm-1 were related to the stretching of Ti-O and bending of O-Ti-O bonds while the vibration mode at 547 cm^{-1} originated from Ni-O bonds [10]. The vibration modes at 631.9 and 760.5 cm^{-1} resulted from stretching vibrations of TiO_6 and octahedral vibrations in the region 500-830 cm^{-1} [11]. In addition, the vibration mode at 227.6 cm^{-1} can result from the asymmetric breathing vibration of the oxygen octahedral. Two vibration modes at 290.2 and 434.3 cm^{-1} can be related to the twist of oxygen octahedral because of vibrations of the Ni and Ti atoms parallel to the xy plane [9].
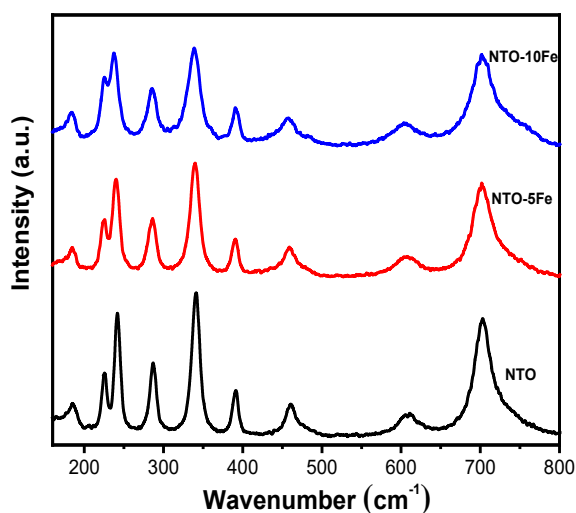

Fig. 2. a), b), c) SEM images of the Fe-doped $NiTiO_3$ and d) EDS spectrum

Fig. 4. Raman spectra of the Fe-doped $NiTiO_3$

The Raman analysis indicated that the ten Raman active modes in synthesized $NiTiO_3$ and Fe-doped $NiTiO_3$ sample confirmed the successful synthesis of materials with ilmenite rhombohedral structure. The shifted peaks in frequency modes at around 240 and 340 cm^{-1} to lower frequencies were suggested for distortion of Ti–O and TiO_6 vibrations due to Fe cations substitution for Ni in host lattice of $NiTiO_3$ materials because Fe cations are smaller than Ni cations. Thus, the XRD and Raman scattering analysis indicated that Fe dopant was well distributed and substituted for Ni in $NiTiO_3$ host crystal.

3.4. Optical Absorbance

Fig. 5 (a) shows the optical absorption spectroscopy of $NiTiO_3$ and Fe-doped $NiTiO_3$ with various Fe concentrations at room temperature. The absorption band can be separated into two ranges around 350-500 nm and 700-900 nm. In addition, the $NiTiO_3$ materials exhibited absorbance peaks at around 380, 454, 504, 740, and 840 nm which correspond to the photon energies of 3.26, 2.73, 2.46, 1.67 eV, and 1.48 eV, respectively. The optical absorption results are in agreement with recently reported for optical properties of $NiTiO_3$ materials where the absorbance peaks resulted from charge transfer from Ni^{2+} to Ti^{4+} because of spin splitting of Ni ions under crystal field. The Fe substitution for Ni-site resulted in suppression of the 504 nm peak which indicated disappearance of charge transfer at 2.46 eV. Moreover, the Fe dopant in $NiTiO_3$ resulted in modification of electronic structure with the absorbance edges of $NiTiO_3$ material tending to shift to visible wavelength with increasing Fe doping concentration. Therefore, we suggested that Fe cation substituted for Ni cation in ilmenite structure resulted in induced new transition.
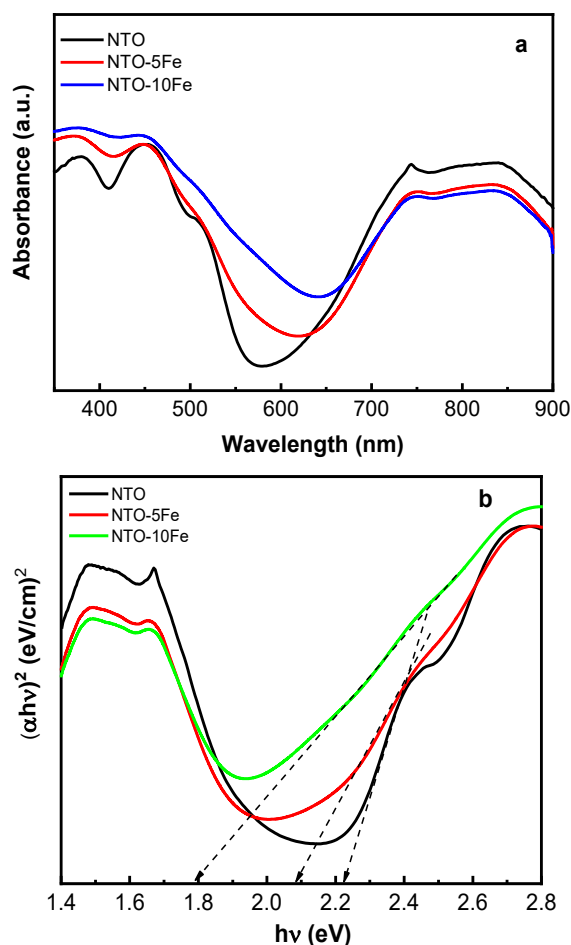

Fig. 5. a) UV-visible absorbance of the Fe-doped $NiTiO_3$ and b) $(\alpha h\nu)^2$ vs. $h\nu$ curve

The optical band gap energy (Eg) was estimated by using the Wood and Tauc method, where Eg values are associated with the absorbance and photon energy by the following equation $(\alpha h\nu) \sim (h\nu\text{-}Eg)^n$, where α is the absorbance coefficient, h the Planck constant, ν the frequency, Eg the optical band gap and n a constant associated with different types of electronic transition. We used $n=1/2$ for direct allowed transition for estimation of the optical band gap energy. The plot of $(\alpha h\nu)^2$ as function of photon energy ($h\nu$) was shown in Fig. 5b. The optical band gap values were estimated from extrapolating linear fitting. For $NiTiO_3$ materials, the largest band gap is expected to relate to the direct electronic transition between the upper edge of O 2p valence band and the lower edge for Ti 3d conduction band. The optical bandgap of pure $NiTiO_3$ samples was 2.23 eV. Our results are consistent with recent observation of the optical band gap of pure $NiTiO_3$ material [12]. The Fe doped $NiTiO_3$ materials resulted in decreasing in optical band gap from 2.23 eV to 1.79 eV for pure $NiTiO_3$ and 10 mol.% Fe substitution for Ni in host $NiTiO_3$, respectively. The modification optical band gap of $NiTiO_3$ materials was recently

reported for doped $NiTiO_3$ materials [4]. In addition, the oxygen vacancies were created due to the unbalance charge between substitution Fe^{3+} ions into host Ni^{2+} ions, resulting reduction in the optical band gap because the state oxygen vacancies are located near the conduction band. Therefore, we suggested that the reduction of optical band gap energy in $NiTiO_3$ materials via Fe-dopants resulted from the new state of Fe ions in the bandgap and/or promotion of oxygen vacancies.

3.5 Analysis of Magnetic Properties

The M-H curves of $Ni_{1-x}Fe_xTiO_3$ (x = 0, 0.05 and 0.10) at room temperature were shown in Fig. 6. Clearly, the Fe dopant samples exhibited the ferromagnetism with typical M-H loops. The pure $NiTiO_3$ sample showed antiferromagnetic behavior with very small remnant magnetization and a negligible coercive field at room temperature. When the Fe dopant concentration increased, the M-H curve changed to ferromagnetic behavior. However, the M-H loops did not reach saturation which suggested the coexistence of ferromagnetism and antiferromagnetism properties.

The ferromagnetic behavior in Fe doped $NiTiO_3$ materials can result from the oxygen vacancies which induced by Fe substituted to Ni in $NiTiO_3$ and formed the interaction between magnetic ions via oxygen vacancies via F-center interaction. The determined saturation magnetization values of 10 mol.% Fe doped $NiTiO_3$ samples can reach 0.482 emu/g. This is significantly higher than that of pure $NiTiO_3$ samples.

3.6. Analysis of Electrical Properties

DC electrical conductivity is one of the useful characterization techniques to understand conductivity mechanism. The variation of DC conductivity of nanocomposites of different Fe dopant with temperature was shown in Fig. 7. It is clear that the conductivity does not vary uniformly with composition. The conductivity of synthesized ceramics depended on the Fe doping concentration and also on the temperature. An increase in conductivity depends on a particular doping concentration. Reports from previous research showed that the conductivity of ilmenite ceramics went up with an increase in temperature. It is seen that, with the rise in temperature, the DC conductivity increases, indicating that the conduction is via a thermally activated process. This shows that both $NiTiO_3$ and Fe doped $NiTiO_3$ exhibit semiconducting behavior. The variation of conductivity with temperature was presented by Arrhenius equation which is given by following:

$$\sigma = A\exp\left(\frac{-E_a}{k_BT}\right) \qquad (2)$$

where A is the pre-exponential factor, E_a is the activation energy, k_B is the Boltzmann constant and T

is the temperature in K. The activation energy was calculated from the slope of Arrhenius plot of $\ln\sigma$ against $(1/T)$.

The activation energy plots of $NiTiO_3$ ceramics with different Fe doping concentration was shown in Fig. 7.
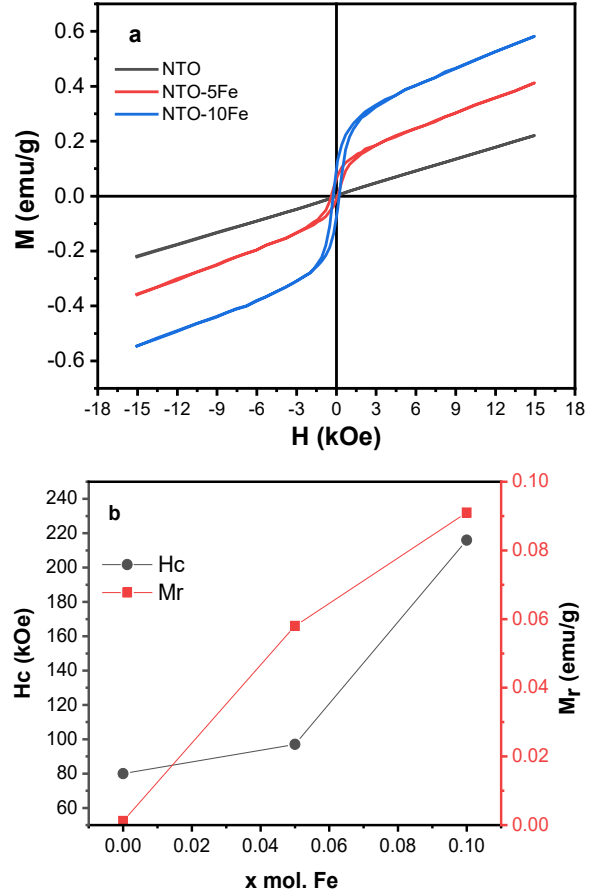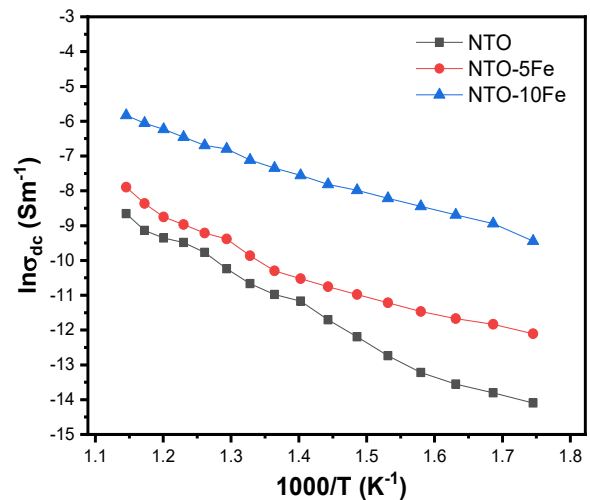

Fig. 6. VSM plots of the Fe-doped $NiTiO_3$

Fig. 7. DC conductivity of the Fe-doped $NiTiO_3$

The activation energy of pure $NiTiO_3$ was 0.82 eV. With changing Fe dopant in $NiTiO_3$ crystal, the activation energy was decreased to 0.56 eV for 5% Fe doping and 0.51 eV for 10% Fe doping. The conductivity of $NiTiO_3$ was higher with increasing Fe doping concentration. This behavior may be due to the Fe dopant which entered the $NiTiO_3$ lattice and enhance the conductivity. Generally, in ferroelectric materials, loss of oxygen often occurred during sintering at higher temperatures, and vacancies are easily created from the lattice considered as the mobile charge carriers. Moreover, the oxygen vacancies can also increase with increasing of Fe dopant. As doping concentration increases the probability of oxygen vacancies can create more, associated with defect formation. During thermal agitation, the oxygen vacancies moved in the lattice and oxide ions are responsible for the electrical conductivity in the prepared ceramic samples.

Table 2. Ferroelectric properties of the $NiTiO_3$ ceramics with the difference in Fe doping

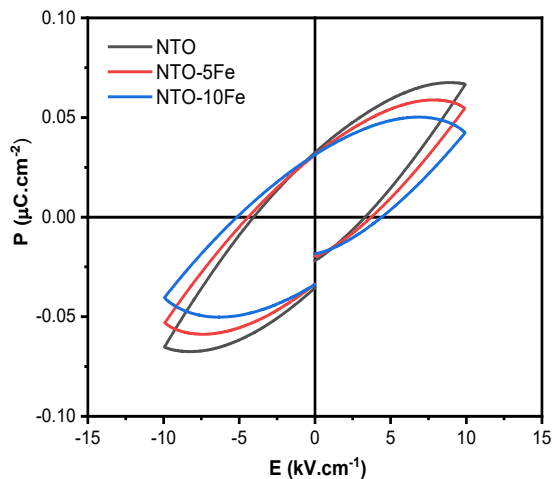| x	P_{max} ($\mu C/cm^2$)	P_r ($\mu C/cm^2$)	E_c (kV/cm)
0	0.072	0.032	3.31
0.05	0.055	0.031	3.72
0.10	0.042	0.031	4.41

Fig. 8. Electric-field-induced-polarization loops of $NiTiO_3$ ceramics as a function of Fe content measured at room temperature

The polarization versus electric field (P-E) curves of $Ni_{1-x}Fe_xTiO_3$ (x = 0, 0.05 and 0.10) at room temperature were presented in Fig. 8. All synthesized samples exhibited the typical loops, confirming the ferroelectric nature of these compounds. The theory revealed that the ferroelectric properties of $NiTiO_3$ ceramic happened in the R3c crystal. However, the R3c phase could not be determined from XRD data

because the structure between the two phases was similar to space group of R-3 and R3c.

It can be seen from P-E loops that the maximum values of polarization of the Fe doped $NiTiO_3$ samples were lower than that of the pure $NiTiO_3$ sample at room temperature. Moreover, the P-E curves of the Fe-doped $NiTiO_3$ samples were lossy behavior which might be attributed to the increase of conductivity with Fe doping. As the discussion in conductivity, the Fe dopant resulted in the increase of conductivity of $NiTiO_3$ sample. Fe dopant can likely act as non-uniform structure which breaks the electric circuit in the presence of applied electric fields. This result indicated that the Fe ion substitution for Ni in $NiTiO_3$ crystal degraded the ferroelectric nature of $NiTiO_3$ and resulted in decreasing in various electrical parameters.

6. Conclusion

The $NiTiO_3$ and Fe-doped $NiTiO_3$ samples were fabricated using sol-gel method. The substitution Fe^{3+} ions into Ni^{2+} ions resulted in decreasing in optical band gap from 2.23 eV to 1.79 eV. The antiferroelectric in $NiTiO_3$ materials was obtained. The Fe doping in $NiTiO_3$ materials induced strong ferromagnetism at room temperature. The Fe substitution for Ni in $NiTiO_3$ lattice increased the electrical conductivity and decreased polarization. Our work was for further understanding the role of interaction in A-site in nanocrystal ilmenite structure for electronic device application.

References

[1] Lihong Yang, Hongmei Qiu, Liqing Pan, Zhengang Guo, Mei Xu, Jinhu Yin,Xuedan Zhao, Magnetic properties of $BaTiO_3$ and $BaTi_{1-x}M_xO_3$ (M=Co, Fe) nanocrystals by hydrothermal method, J. Magn. Magn. Mater. 350 (2014) 1–5.
https://doi.org/10.1016/j.jmmm.2013.09.036

[2] B. Xu, K.B. Yin, J. Lin, Y.D. Xia, X.G. Wan, J. Yin, X.J. Bai, J. Du, Z.G. Liu, Room-temperature ferromagnetism and ferroelectricity in Fe-doped $BaTiO_3$, Phys. Rev. B. 79 (2009) 134109.
https://doi.org/10.1103/PhysRevB.79.134109

[3] A. Karaphun, S. Hunpratub, E. Swatsitang, Effect of annealing on magnetic properties of Fe-doped $SrTiO_3$ nanopowders prepared by hydrothermal method, Microelectron. Eng. 126 (2014) 42–48.
https://doi.org/10.1016/j.mee.2014.05.001

[4] Y. Lin, Y., Chang, Y., Chen, G., Chang, Y., and Chang, Y. Lin, Effects of Ag-doped $NiTiO_3$ on photoreduction of methylene blue under UV and visible light irradiation, J. Alloy. Compd. J. 479 (2009) 785–790.
https://doi.org/10.1016/j.jallcom.2009.01.061

[5] S. Yuvaraj, V.D. Nithya, K.S. Fathima, C. Sanjeeviraja, G.K. Selvan, S. Arumugam, R.K. Selvan, Investigations on the temperature dependent electrical and magnetic properties of $NiTiO_3$ by molten salt synthesis, Mater. Res. Bull. 48 (2013) 1110–1116. https://doi.org/10.1016/j.materresbull.2012.12.001

[6] Y. Fujioka, J. Frantti, A. Puretzky, G. King, Raman Study of the structural distortion in the $Ni_{1-x}Co_x$ TiO_3 solid solution, Inorg. Chem. 55 (2016) 9436–9444. https://doi.org/10.1021/acs.inorgchem.6b01693

[7] N. Lenin, A. Karthik, M. Sridharpanday, M. Selvam, S.R. Srither, S. Arunmetha, P. Paramasivam, V. Rajendran, et al Lenin, N., Karthik, A., Sridharpanday, M., Selvam, M., Srither, S. R., Arunmetha, S., Electrical and magnetic behavior of iron doped nickel titanate ($Fe^{3+}/NiTiO_3$) magnetic nanoparticles, J. Magn. Magn. Mater. 397 (2016) 281–286. https://doi.org/10.1016/j.jmmm.2015.08.115

[8] M.I. Baraton, G. Busca, M.C. Prieto, G. Ricchiardi, V.S. Escribano, On the Vibrational Spectra and Structure of $FeCrO_3$ and of the Ilmenite-Type Compounds $CoTiO_3$ and $NiTiO_3$, J. Solid State Chem. 112 (1994) 9–14. https://doi.org/10.1006/jssc.1994.1256

[9] M.A. Ruiz Preciado, A. Kassiba, A. Morales-Acevedo, M. Makowska-Janusik, Vibrational and electronic peculiarities of $NiTiO_3$ nanostructures inferred from first principle calculations, RSC Adv. 5 (2015) 17396–17404. https://doi.org/10.1039/C4RA16400H

[10] R. Vijayalakshmi, V. Rajendran, Effect of reaction temperature on size and optical properties of $NiTiO_3$ nanoparticles, E-Journal Chem. 9 (2012) 282–288. https://doi.org/10.1155/2012/607289

[11] K.P. Lopes, L.S. Cavalcante, A.Z. Sim, J.A. Varela, E. Longo, E.R. Leite, $NiTiO_3$ powders obtained by polymeric precursor method: Synthesis and characterization, J. Alloys Compd. 468 (2009) 327–332. https://doi.org/10.1016/j.jallcom.2007.12.085

[12] P.H.M. de Korte, G. Blasse, Water photoelectrolysis using nickel titanate and niobate as photoanodes, J. Solid State Chem. 44 (1982) 150–155. https://doi.org/10.1016/0022-4596(82)90359-0